Journal of Applied Fluid Mechanics, Vol. 12, No. 4, pp. 1013-1021, 2019.
Available online at www.jafmonline.net, ISSN 1735-3572, EISSN 1735-3645.
DOI: 10.29252/jafm.12.04.29280

Numerical Investigation of Influence of Flow Rates on Combustion Characteristics using Multiphase Flamelet Combustion

N. Shreekala† and S. N. Sridhara

Visvesvaraya Technological University 2, Belgaum, Karnataka, 590018, India

†*Corresponding Author Email: shreekala.n@gmail.com*

(Received June 15, 2018; accepted November 11, 2018)

ABSTRACT

Numerical analysis plays vital role in designing gas turbine combustors for improving its performance. It requires deep understanding of turbulent and multiphase reactive flow physics inside the combustor. Hence present work focusses on numerical investigation of turbulent flow and reactive interaction between liquid spray of aviation kerosene droplets and air for the experimentally investigated combustor configuration. The present analysis results agree well with the experimental test results. Mixture fraction based Probability Density Function flamelet combustion model is used to solve transport equations by generating the flamelet library for Jet-A fuel. The analysis provides good insight into the multiphase combustion process and the flow phenomena occurring inside the combustor. Further, combustion performance characteristics at different design point operations are investigated in the present work keeping the air fuel ratio constant. Results show rise in peak velocity by 2.5 times and pressure loss factor by 6 for design point operating at higher flow rates in comparison with the baseline design operating point.

Keywords: Mass flow rate; Mixture fraction; Performance parameter; Pattern factor; Pressure loss.

NOMENCLATURE

A_o	discharge orifice area	PDF	Probability Density Function
A_p	total inlet ports area	TAF	Total Air Flow
D_S	swirl chamber diameter	$\dot{m}_L$	mass flow rate
d_o	diameter of discharge orifice	ΔP	pressure differential
FN	flow Number	ρ_L	liquid density

1. INTRODUCTION

In the recent years with the increase in the air traffic and stringent emission norms, more thrust is given on clean emissions. Important factors to control emission are considered in terms of equivalence ratio, temperature, residence time and degree of homogeneity in primary zone and spray characteristics of the fuel (Lefebvre, 2013). Carbon Monoxide (CO) and Unburned Hydro Carbons (UHC) in the exhaust gases pose the major source of pollutant emissions. Incomplete combustion leads to these emissions. Effective mixing of fuel and air with optimum equivalence ratio of around 0.8 in primary zone is required for lower emissions. Various studies have been conducted to improve combustor performance by taking several steps to aim complete combustion of the fuel. Fuel injection and its spray characteristics is one of the key factor in improving efficiency and performance of the gas turbine combustor.

Several studies have been conducted on practical gas turbine combustors to understand the relevant physical phenomena occurring inside the combustors. Jones *et al.* (1983) experimentally investigated the gaseous propane combustion in a research gas turbine combustion chamber and measured temperature and concentrations of combustion products. He also showed reduction of levels of emission and unburnt hydrocarbons with the increase in inlet temperature. Similar study on measurement of combustion characteristics by finding the effect of intensity of swirl on propane in a turbulent non-premixed flame is done by Ji-Hyun

Kwark *et al.* (2004). However majority of the industrial furnaces, diesel engines and aero applications use more fuel efficient and less polluted spray combustion. Complex atomizers are involved for generating spray into finer droplets which improves combustion efficiency. Ghaffarpour *et al.* (1993) and Jones *et al.* (1991) conducted experiments on kerosene spray combustion. Ghaffarpour *et al.* (1993) measured the kerosene spray velocity and droplet size distributions using Phase Doppler Particle Analyser (PDPA) and investigated the effect of inlet air flow rates on flame stability whereas Jones *et al.* (1991) measured temperature and combustion gas concentrations inside combustor for two air fuel ratios. However majority of the experimental works performed for years serves as benchmark for the computational works validation. Further to reduce the overall cost and time involved in performing experiments and to gain insight of the complex flow phenomena, CFD tool plays a promising role in design modifications and performance improvement of the combustors. Zamuner *et al.* (2002) numerically simulated the reactive kerosene spray combustion using in-house built numerical code to study the turbulent flow physics inside the realistic gas turbine combustor and studied the effect of increase in swirl number on radial temperature distribution at the combustor exit. Sharma *et al.* (2004 and 2001) developed a stochastic separated flow computational model to show the influence of fuel volatility and liquid spray parameter on combustion efficiency and emission characteristics. He showed droplet penetration reduces with the increase in spray cone angle, inlet pressure and air swirl. Subsequent numerical optimization study of gas turbine combustor mixing is performed for improving exit temperature profile by Oboetswe S. Motsamai *et al.* (2010). Further Zhang *et al.* (2017) worked on various combustion models to study the turbulent combustion in non-premixed and premixed combustion in a realistic tay combustor. In the latest study by Parag Rajpara *et al.* (2018), large eddy simulations are performed for conventional and reverse flow CAN combustors to demonstrate the energy required for combustor wall cooling and compared exit temperature and NO_x emission for both the cases. In a parallel study Alemi *et al.* (2017) numerically investigated the injection diameter and direction of the jet for reducing the NO emission for different Reynolds number.

Several experimental and numerical investigations are being performed to find the effect of varying air fuel ratio (AFR) on combustion characteristics. However less studies have been made on influence of increasing mass flow rates of air and fuel on combustion characteristics keeping AFR constant, considered as design point operations here.

2. GOVERNING EQUATIONS

The continuity, momentum and energy equations along with species transport equations are given below

$$\frac{\partial \rho}{\partial t}+\frac{\partial(\rho U_i)}{\partial x_j}=S_m \tag{1}$$

$$\frac{\partial U_i}{\partial t}+\sum_j U_j\frac{\partial U_i}{\partial x_j}=-\frac{1}{\rho}\frac{\partial P}{\partial x_j}+\sum_j\frac{1}{\rho}\frac{\partial \tau_{ji}}{\partial x_j}+g_i+S_p \tag{2}$$

$$\frac{\partial(\rho c_p T)}{\partial t}+U_j\frac{\partial(\rho c_p T)}{\partial x_j}=K\frac{\partial^2 T}{\partial x_i \partial x_j} - P\frac{\partial U_i}{\partial x_j}+\tau_{kj}\frac{\partial U_k}{\partial x_j}+S_T \tag{3}$$

$$\frac{\partial C_n}{\partial t}+U_j\frac{\partial C_n}{\partial x_j}=\frac{\partial}{\partial x_j}\left(D_n\frac{\partial \tau_n}{\partial x_j}\right)+S_n \tag{4}$$

The source terms S_m, S_p, S_T and S_n represents the particles for mass, momentum, energy and species concentration respectively. The terms on left hand side in the above equations represents conservative properties such as accumulation and advection respectively. In the energy equation, the term with thermal conductivity K represents heat transfer. The right hand side of the last equation represents species transport which is due to molecular diffusion of the species.

2.1 Governing equation for fuel evaporation

Spray combustion includes liquid evaporation, droplet formation, interphase heat and mass transfer between liquid and gaseous phases. In the present case pressured liquid is forced through the nozzle orifice for atomization of fuel. During atomization the liquid fluid gets dissipated into small droplets. Fuel and injector properties control the atomization process. The size of the droplet determines the time required for its evaporation and combustion given by D^2 law.

$$D^2(t)=D_0^2-Kt \tag{5}$$

Using the above Eq. (5) the droplet life is given by

$$t_d=D_0^2/K \tag{6}$$

Where K is the evaporation constant, $D^2(t)$ is the variation of the droplet diameter as a function of time, D_0 is the initial droplet diameter.

Spray simulation involves comprehensive model generation involving complex interdependent processes. Raoult's law is applied for fuel evaporation to obtain equilibrium between the liquid and gaseous phases.

2.2 Governing equation for Fuel Distribution

In addition to mean droplet size, another important parameter in defining spray is the distribution of fluid particles. For liquid sprays most widely used and convenient way of representation is Rosin Rammler distribution of droplets. The distribution assumes exponential relationship between droplet diameter (d) and mass fraction (Y_d) of droplets having diameter greater than d

$$Y_d = e^{-(d/\bar{d})^n} \tag{7}$$

Where $\bar{d}$ represents the mean diameter and n as the spread parameter.

3. Design Calculation For Nozzle Pressure Differential And Exit Velocity

Pressurised liquid is injected through a simple nozzle orifice of the Pressure atomizer. With smaller orifice, fine atomization can be obtained. The effective flow area of the atomizer is described in terms of flow number.

$$FN = \frac{(\dot{m}_L)}{\sqrt{(\Delta P)\times(\rho_L)}} \tag{8}$$

The coefficient of discharge is the ratio of actual to theoretical mass flow rates. The discharge coefficient takes into account the losses incurred in the flow passages of the nozzle. Its relation with the nozzle flow rate is given by

$$C_D = \frac{m_L}{A_0\sqrt{\rho_L \Delta P}} \tag{9}$$

But according to experimental results by Rizk *et al.* (1985) the discharge coefficient is also given by

$$C_D = 0.36\sqrt{\left(\frac{A_P}{D_S d_o}\right)\left(\frac{D_S}{d_o}\right)} \tag{10}$$

Combining Eqs. (8), (9) and Eq. (10) the Flow Number (FN) in terms of the dimensions of pressure swirl atomizer is given by

$$FN = 0.389 d_0^{1.25} A_p^{0.5} D_S^{-0.25} \tag{11}$$

Several experiments have been conducted to obtain the relation between spray cone angle and atomizer dimensions. Taylor (1948) in his experiments showed that spray cone angle solely depends on atomizer dimensions and is a function of $\left(\frac{A_P}{D_S d_o}\right)$.

This ratio is obtained from the chart for the spray cone angle of 70^0. The discharge coefficient for this value is obtained from the chart "Relationship between discharge coefficient and atomizer dimensions" (Lefebvre, 2013) for the graph $\left(\frac{D_S}{d_o}\right) = 5$. Considering the values of the parameters obtained from the graphs above and substituting the values in the flow number equations, the pressure drop across the nozzle is calculated. This forms the major input parameter to calculate the discharge velocity from the nozzle orifice.

The velocity of the fluid at the tip of the atomizer is given by

$$V_F = \sqrt{\left(\frac{2\Delta P}{\rho_L}\right)} \tag{12}$$

Henceforth the velocity calculated by the above procedure is used as input parameter in the present analysis.

4. Combustion Configuration

The flow configuration and boundary conditions used for simulation resembles the configuration experimentally investigated by Jones *et al.* (1991). Figure 1 shows the schematic model of the gas turbine CAN combustor typically used in aircraft engines, being used in the present study. Combustion chamber of 75 mm diameter consists of six equally spaced primary holes of size 10 mm diameter and dilution holes of size 20 mm diameter staggered placed around the combustion chamber circumferentially. $1/6^{th}$ of the model is numerically analysed in the present study for reducing computational effort due to symmetry of the geometry.

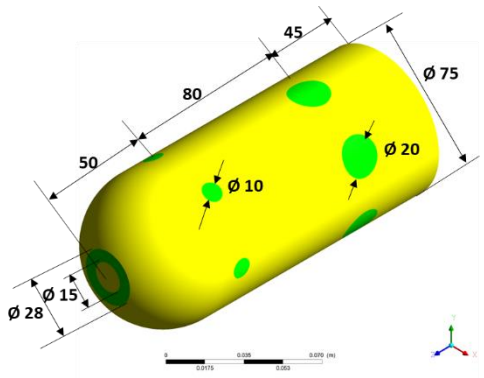

All dimensions in mm only

Fig. 1. Schematic full model of gas turbine CAN combustor.

5. Numerical Setup And Boundary Conditions

Figures 2 and 3 shows the sector model and the boundary conditions specified for the present case. The combustion chamber is numerically represented by computational domain made of 928,865 tetrahedral and 89,632 wedge cells totalling 1,018,497 elements. 60^0 sector model with periodic boundary conditions is created for reducing computational effort. Boundary flow is captured by modelling 5 boundary layer cells with near wall cell thickness of 0.1 mm. Mesh sizing is done using local biased seeding based on the flow region. The mesh quality parameters are checked and maintained within allowable limits to obtain accurate results. Steady state, turbulent reacting flow analysis is performed solving three-dimensional governing equations. The relative mass flow through the swirler, primary holes and dilution holes are maintained as given by Jones *et al.* (1991).

Air fuel ratio of 57 considered for the present study is as used by the Jones *et al.* (1991). Total air supply of 0.1 kg/s is preheated to 400 K before entering the combustor. The air is distributed with 9.9% through

swirler, 13.7% through the primary holes and 58% through the secondary holes called dilution holes and remaining for barrel cooling. An initial swirl of 45^0 is provided by the swirler at the inlet. Non-swirling hollow cone spray of fuel with an included angle of 70^0 is sprayed concentric with swirler. The fuel atomization results in breakup of fluid into numerous non zero size droplets. When cohesive surface tension force increases, the droplets size reduces leading to distribution of different size of fuel droplets. In the present case assumption of Rosin Rammler distribution is made which is widely used for droplet distribution with sauter mean diameter of 50 microns.

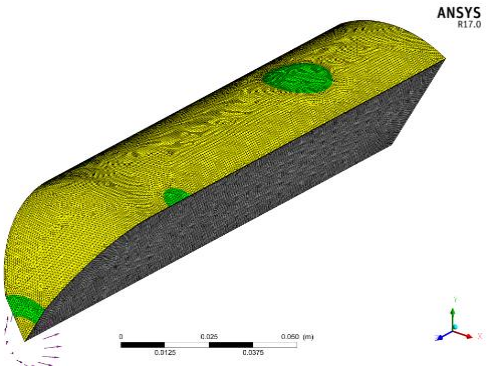

Fig. 2. 60^0 sector of tetrahedral meshed model of CAN combustor.

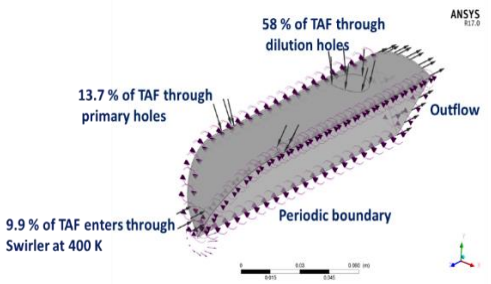

Fig. 3. Model showing boundary conditions.

Complete combustion reaction modeling is used with full NOx. Laminar flamelet with Probability Density Function (PDF) is used to solve transport equations with high scalar dissipation rate. The required Flamelet library is generated using Jet-A aviation fuel as the fuel module and particle transport combustion model with PDF is used. The coupling of laminar chemistry with fluctuating turbulent flow field is done by solving PDF transport equations. The generated Flamelet library provides scalar dissipation rate, mixture fraction variance and mean species mass fractions as functions of mean mixture fraction. Flamelet library file created provides table containing mass fraction of the individual component as a function of mean mixture fraction. Combustion analysis is performed using PDF Flamelet which is a mixture fraction based combustion model in concurrence with flamelet library.

Fuel is modelled with Lagrangian (particle transport) approach. These fuel particles are fully coupled with the continuous gaseous phase. This helps in continuous exchange of momentum between fuel and air to predict the effect of fuel particles on gaseous phase at the cost of higher computational cost compared to one way coupling. Schiller-Naumann drag model calculates the interphase drag force and Ranz Marshall heat transfer model enables the transfer of heat between the air and the fuel particles.

Figure 4 depicts the pictorial representation of the fuel and air inputs into the combustor with different colour coding. The grey colour lines depicts the swirler air entering into combustor. It appears that the swirler air spreads and closely follows the combustor walls in the dome region. The pink and green colour lines represent the primary and secondary air entering into combustor. The blue colour lines represent the liquid fuel sprayed inside and mixing with the primary and secondary air.

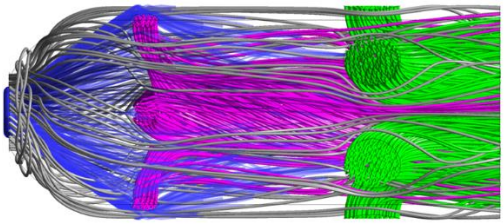

Fig. 4. Plot depicting the air and fuel flowing through inlets.

6. RESULTS AND DISCUSSION

6.1 Baseline Analysis (Design Point 1)

The contour plots of Mixture fraction and CO_2 mass fraction distribution for the baseline design point is shown in Figs. 5 and 6. These plots depicts the overview of the flow pattern inside combustor. Figures 5(a) and 6(a) shows mixture fraction and CO_2 contours along the plane passing between primary holes and passing through dilution hole whereas Figs. 5(b) and 6(b) display contours along the plane passing through primary holes. These plots illustrate the turbulent and reactive flow phenomena and combustion species distribution inside the combustor.

The coaxial swirling flow of air mixes with the injected fuel spray in the dome and travels tangentially towards the wall of the combustor. This mixture interacts with the primary air, reverses its flow, leading to the formation of a small pocket of recirculation zone ahead of primary hole. This zone is rich in fuel attributing to insufficient availability of oxygen from swirl air input resulting in higher mixture fraction in this pocket as seen in Fig. 5(a&b). Also the combustion gases in the upstream of the combustor near the inlet will be rich in CO

concentration due to unavailability of sufficient oxygen for the combustion to take place as seen in Fig. 7. Impingement of primary jet of air, dilutes the fuel air mixture downstream and near the centreline of the combustor, accelerating the hot combustion gases axially. However entrainment of large amount of cooling air through the dilution holes cuts the axial flow of the combustion gases leading to the formation of large recirculation zone in the secondary region of the combustor. This characterises higher level of turbulence by generating low pressure zone at the centre and providing sufficient time for complete combustion thereby playing significant role in flame stabilization. Consequently the accelerating hot gas mixture in the recirculation zone influences the dilution jets to bend downstream. At the same time the accelerating hot gases near the combustor wall is obstructed by the dilution jets creating flow reversal leading to formation of a small pocket of clockwise high temperature recirculation zone in this region. This can be observed clearly for all design points in Fig. 11. Significant temperature differential between the hot gases and cooler dilution air enhances mixing rate and combustion rate justifying higher concentration of CO_2 in the region as shown in Fig. 6. Similar phenomena of high temperature region occurs near the centreline in the plane bisecting the primary holes zone wherein mixing rate is increased in the presence of primary jet of air shown in Fig. 11.

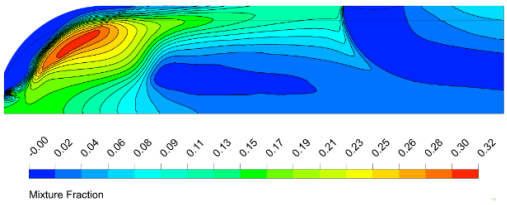

Fig. 5 (a). Contour plot of Mixture fraction along the plane passing through dilution hole.

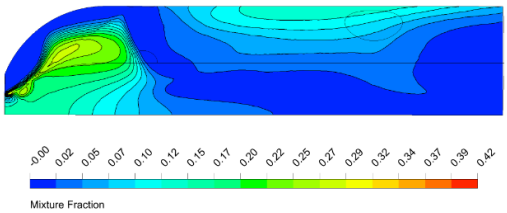

Fig. 5 (b). Contour plot of Mixture fraction along the plane passing through primary hole.

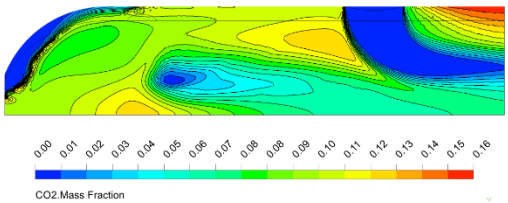

Fig. 6 (a). Contour plot of CO_2 mass fraction along the plane passing through dilution hole.

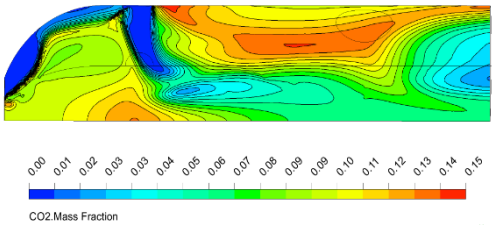

Fig. 6 (b). Contour plot of CO_2 mass fraction along the plane passing through primary hole.

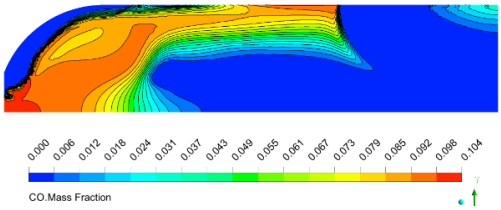

Fig. 7. Contour plot of CO mass fraction along the plane passing through dilution hole.

The numerically predicted mixture fraction values are validated with the experimental work conducted by Jones *et al.* (1991) on a model CAN combustor. Figure 8 shows the comparison graph of experimental radial variation of mixture fraction values at different sections with the present analysis. The model predictions of radial variation of the mixture fraction agree very well at x = 30 mm (primary zone) and x = 90 mm (secondary zone) whereas predictions slightly overestimate at x = 50 mm (primary hole location) however capturing the radial variation trend well with the experiments. Insufficient information on geometrical and spray data in the experimental work forced to make assumptions leading to variation in the analysis results at certain locations.

The value of mixture fraction is around 0.32 near the hollow cone exit as seen in Fig. 5(a) reduces drastically to 0.13 in the primary zone visible in Fig. 8. Also radial peak mixture fraction values and centreline mixture fraction values reduce with the axial advancement of the combustion gas mixture. This can be attributed to greater mixing subsequent to formation of recirculation pockets in the mid region between axis and wall of the combustor. With the entrainment of primary and dilution jet of air, fuel percentage in the hot gas mixture reduces gradually ensuring sufficient supply of oxygen for combustion indicating the reduction of unburnt fuel in the burnt gases in the downstream region.

Figure 9 depicts the variation of species concentrations of CO_2, CO, NO and O_2 radially at different axial locations. The profile in primary zone (x = 30 mm) indicates higher CO concentrations and reduces at stations downstream with inverse trends observed in NO concentrations since primary zone is fuel rich and nitrogen deficient region. CO mass fraction chart shows its concentration almost nil at the exit. Further the peak NO mass fraction values are seen along the centreline and wall of the combustor at the exit. Consistent increase in oxygen concentration at

downstream stations are observed indicating adequate supply of air for complete burning of fuel. Also at the exit, minimum CO_2, CO and NO mass fractions are observed at half the radius and reverse trend in oxygen concentration is observed at the exit along dilution jet plane.

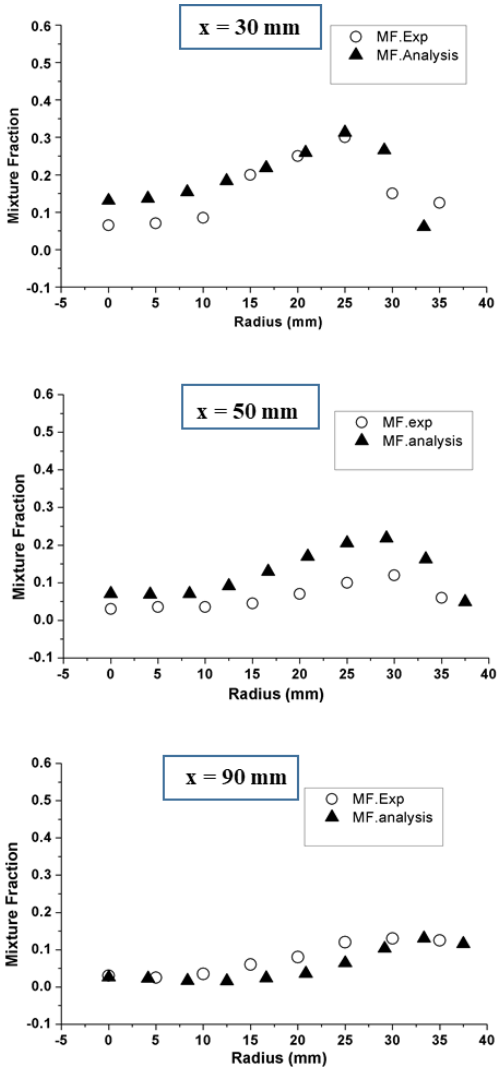

Fig. 8. Variation of mixture fraction radially at different axial locations along dilution jet plane: comparison between experimental and computation.

6.2 Comparison of Design Operating Points

Various studies have been performed to investigate the effect of design points operating at higher air and fuel flow rates on combustor performance keeping the air fuel ratio constant of 57. Table 1 shows the air and fuel mass flow rates considered for the design operating points.

Effect of air and fuel mass flow rates operating at various design points (DP) on the combustion parameters is studied in the present analysis. Figure 10 gives the comparison of the peak mixture fraction values for the design points studied. These peak mixture fraction values are observed at x = 30 mm in the primary region for all the operating design points. Analysis shows amount of air entering the swirler increases with the operating design points showing higher mixing rate, subsequently reducing the peak mixture fraction values from 0.32 for baseline analysis to 0.23 for DP 4. Whereas overall flow pattern remains the same for all the design studies. In case of temperature and velocity plots, the impact of changes in air and fuel mass flow rates is clearly visible.

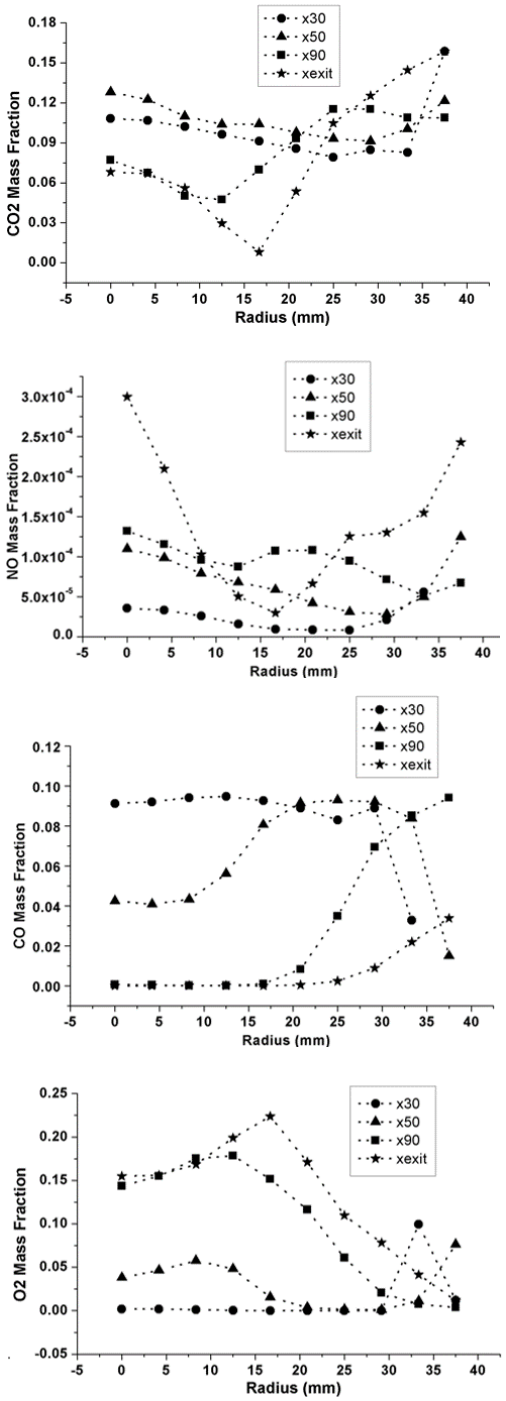

Fig. 9. Radial variations of species concentrations at axial locations x =30 mm, x = 50 mm, x = 90mm and exit along the dilution jet plane.

Table 1 Inlet mass flow rates of air and fuel for the operating design points

Design Points	Fuel mass flow rate (kg/s)	Air mass flow rate (kg/s)
Design point 1 (Baseline analysis)	0.00175	0.1
Design point 2	0.00263	0.15
Design point 3	0.00351	0.2
Design point 4	0.00438	0.25

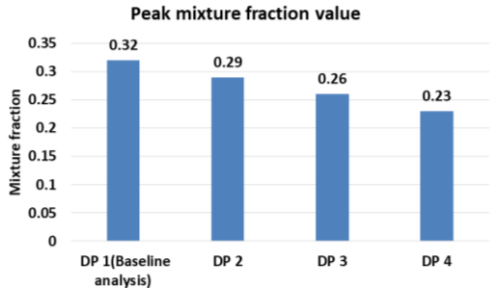

Fig. 10. Chart showing the peak mixture fraction value along the dilution jet plane for the operating design points.

The analysis suggests, there is a shift in the pocket of burnt gases comprising hot gases identified near the centreline at x = 50 mm towards upstream. Increase in the intensity of recirculation near the fuel injector and rise in cross-flow primary air together carries hot combustion gases towards inlet of the combustor with enhanced flow rates. These are clearly visible in Fig. 11 depicting temperature contour plots along the plane passing through dilution jets. It is visible from these plots, major chunk of reactive mixing of fuel and air occurs in the secondary zone with the occurrence of intense central recirculation due to the formation of large blockage of the dilution jets for axial flow. However downstream flow pattern is influenced predominantly by dilution jets wherein reaction plays minor role in this region. Corner recirculation zones are avoided in this profile geometry of the combustor.

Figure 12 depicts the velocity vector plots for all the four operating design points. The velocity plots show surge in the hot combustion gases downstream of the dilution jets. The region between dilution holes acts as nozzle resulting in velocity augmentation. Henceforth Peak velocities are found in this region. The velocity crest increases from 55 m/s for the baseline analysis to 140 m/s for design point 4 operating at higher flow rates.

Table 2 provides the comparison of the average values of mass fraction of the baseline analysis with the other design points at the exit of the combustor. It can be observed that smaller traces of fuel is found at the exit, reducing further with design points operating at higher flow rates. This ensures effective reactive mixing occurring in the combustor configuration studied in the present work. The lower NO mass fraction is seen for all the operating design points with further reduction seen in higher flow rate design points. It appears from the graph that increase in air and fuel flow rates showing reduction trend in pollutant combustion species and unburnt fuel ensuring increase in mixing efficiency.

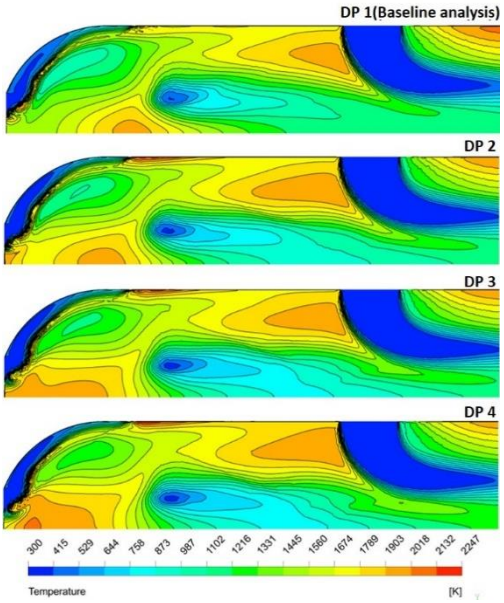

Fig. 11. Comparison of the temperature contour plots along the dilution jet plane for the operating design points.

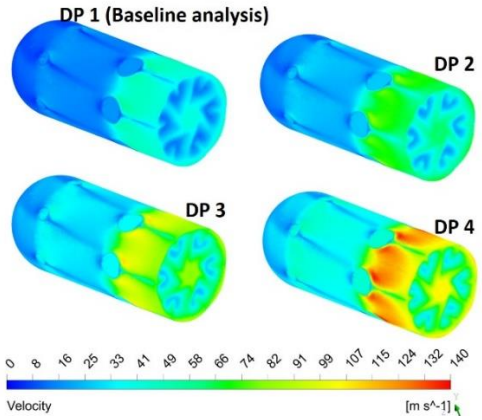

Fig. 12. Comparison of the velocity vector plots for the operating design points.

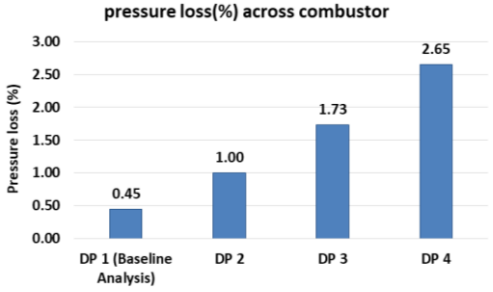

Fig. 13. Chart showing the pressure loss factor (%) for the operating design points.

Figure 13 shows the bar chart depicting the pressure loss percentage across combustor for all the design

Table 2 Average mass fraction of combustion species at the exit for the operating design points

Design Points	Mass fraction				
	NO	CO	CO_2	H_2O	$C_{10}H_{22}$
DP 1 (Baseline Analysis)	8.67 E-05	1.25 E-02	7.41 E-02	3.31 E-02	1.09 E-07
DP 2	7.68 E-05	1.06 E-02	7.42 E-02	3.24 E-02	5.6 E-08
DP 3	7.15 E-05	7.74 E-03	7.24 E-02	3.06 E-02	1.11 E-08
DP 4	6.807 E-05	7.15 E-03	7.16 E-02	3.00 E-02	8.08 E-09

points. The baseline analysis shows 0.45% pressure loss percentage across combustor increasing to 2.65% for the design point 4. There is a steady increase in pressure loss with the increment in air and fuel flow rates. This attributes to irreversible combustor heating with mixing enhancement thereby creating turbulence and frictional losses caused by working fluid. Even though minimum pressure loss is the basic requirement of the combustor, eliminating these losses is not possible which aids better mixing.

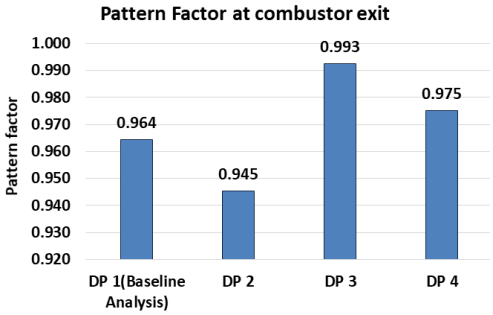

Fig. 14. Chart showing the Pattern Factor for the operating design points.

Figure 14 depicts the chart showing the pattern factor at the exit. Pattern factor assesses the mixing effectiveness at the exit of the combustor. The present model analysis shows pattern factor values which needs improvement. This will be done in our future work. With the current study DP 2 shows better pattern factor compared to other operating design points.

7. CONCLUSION

Reactive flow analysis of a gas turbine CAN combustor with swirling air input is numerically investigated. The analysis provides good insight into the multiphase combustion process and flow phenomena occurring inside the combustor. The analysis results agree closely with the experimental tests and variations are within the permissible limit.

Higher concentrations of mixture fraction and CO with the value of 0.32 and 0.1 mass fraction respectively is observed in the primary zone. However oxidation of carbon monoxide in the downstream region occurs with the entrainment of primary and secondary air ensuring chemical equilibrium state, showing secondary and dilution zone rich in CO_2.

Peak mixture fraction of 0.32 is observed in the baseline analysis. But with the increase in air and fuel flow rates, peak mixture fraction value reduces to 0.23 in design point 4. This ensures better mixing with the enhancement of flow rates. However there is no change in the flow behavior for all the design operating points.

Increase in the flow rates of reactant mixture produces large quantity of hot combustion gases moving with higher velocities. Hence design point 4 peak velocity increases by 2.5 times and pressure loss factor across combustor by 6 times in comparison with the baseline analysis. Also there is a steady decrement in the exit NO, CO and fuel mass fractions with studied operating points from baseline to DP 4.

REFERENCES

Alemi, E. and M. Rajabi Zargarabadi (2017). Effects of jet characteristics on NO formation in a jet-stabilized combustor. *International Journal of Thermal Science* 112, 55-67.

Ghaffarpour, M. and B. Chehroudi (1993). Experiments on Spray Combustion in a Gas Turbine Model Combustor. *Combustion Science and Technology* 92(3), 173-200.

Ji-Hyun K., J. Yong-Ki and J.Chung-Hwan (2004). Effect of Swirl Intensity on the Flow and Combustion of a Turbulent Non-Premixed Flat Flame. *Flow Turbulence and Combustion* 73(4), 231-257.

Jones, W. P. and A. Tober (1991). Measurements of Gas Composition and Temperature inside Can Type Model Combustor. *International Union of Theoretical and Applied Mechanics, IUTAM Symposium Taipei, Taiwan*, 327-338.

Jones, W. P. and H. Toral (1983). Temperature and Composition Measurements in a Research Gas Turbine Combustion Chamber. *Combustion Science and Technology* 31(6), 249-275.

Lefebvre, A. H. and Dilip R. Ballal (2013). *Gas*

turbine combustion: Alternative fuels and emissions, Third edition. Hemisphere Publishing Corporation, London, New York.

Oboetswe, S., Motsamai, Jan A. Snyman and Josua P. Meyer (2010). Optimization of Gas Turbine Combustor Mixing for Improved Exit Temperature Profile. *Heat Transfer Engineering, Taylor and Francis group* 31, 402-418.

Parag, R., A. Dekhatawala, R. Shah and J. Banerjee (2018). Thermal and emission characteristics of reverse air flow CAN combustor. *International Journal of Thermal Sciences* 128, 175-183.

Rizk, N. K. and A. H. Lefebvre (1985). Internal Flow Characteristics of Simplex Swirl Atomizers. *Journal of Propulsion and Power* 1, 93-199.

Sharma, N. Y. and S. K. Som (2004). Influence of fuel volatility and spray parameters on combustion characteristics and NOx emission in a gas turbine combustor. *Applied Thermal Engineering* 24, 885-903.

Sharma, N. Y., A. Datta and S. K. Som (2001). Influences of spray and operating parameters on penetration of vaporizing fuel droplets in a gas turbine combustor. *Applied Thermal Engineering* 21, 1755-1768.

Taylor, G. I. (1948). The Mechanics of Swirl Atomizers. *Seventh International Congress of Applied Mechanics* 2, 280-285.

Zamuner, B., P. Gilbank, D. Bissières and C. Berat (2002). Numerical simulation of the reactive two-phase flow in a kerosene/air tubular combustor. *Aerospace Science and Technology* 6, 521-529.

Zhang, K., A. Ghobadian and J. M. Nouri (2017). Comparative study of non-premixed and partially-premixed combustion simulations in a realistic Tay model combustor. *Applied Thermal Engineering, Elsevier* 110, 910-92.